



A Journal of the Gesellschaft Deutscher Chemiker

Angewandte Chemie

GDCh

International Edition

www.angewandte.org

Accepted Article

Title: Generating Defect-Rich Bismuth for Enhancing Rate of Nitrogen Electroreduction to Ammonia

Authors: Yue Wang, Miao-miao Shi, Di Bao, Fan-lu Meng, Qi Zhang, Yi-tong Zhou, Kai-hua Liu, Yan Zhang, Jia-zhi Wang, Zhi-wen Chen, Da-peng Liu, Zheng Jiang, Mi Luo, Lin Gu, Qing-hua Zhang, Xing-zhong Cao, Yao Yao, Min-hua Shao, Yu Zhang, Xin-Bo Zhang, Jingguang G. Chen, Jun-min Yan, and Qing Jiang

This manuscript has been accepted after peer review and appears as an Accepted Article online prior to editing, proofing, and formal publication of the final Version of Record (VoR). This work is currently citable by using the Digital Object Identifier (DOI) given below. The VoR will be published online in Early View as soon as possible and may be different to this Accepted Article as a result of editing. Readers should obtain the VoR from the journal website shown below when it is published to ensure accuracy of information. The authors are responsible for the content of this Accepted Article.

To be cited as: *Angew. Chem. Int. Ed.* 10.1002/anie.201903969
Angew. Chem. 10.1002/ange.201903969

Link to VoR: <http://dx.doi.org/10.1002/anie.201903969>
<http://dx.doi.org/10.1002/ange.201903969>

Generating Defect-Rich Bismuth for Enhancing Rate of Nitrogen Electroreduction to Ammonia

Yue Wang^{a,†}, Miao-miao Shi^{a,†}, Di Bao^{b,†}, Fan-lu Meng^{a,†}, Qi Zhang^b, Yi-tong Zhou^a, Kai-hua Liu^a, Yan Zhang^a, Jia-zhi Wang^b, Zhi-wen Chen^a, Da-peng Liu^c, Zheng Jiang^e, Mi Luo^e, Lin Gu^f, Qing-hua Zhang^f, Xing-zhong Cao^g, Yao Yao^h, Min-hua Shao^h, Yu Zhang^c, Xin-Bo Zhang^b, Jingguang G. Chen^{d,*}, Jun-min Yan^{a,*}, Qing Jiang^a

Abstract: The electrochemical N₂ fixation, which is far from practical application in aqueous solutions under ambient conditions, is extremely challenging and requires rational design of electrocatalytic centers. Herein, we observed that semimetal bismuth (Bi) might be a promising candidate because of its poor binding with H-adatoms for increasing the selectivity and production rate, and successfully synthesized defect-rich Bi nanoplates as an efficient noble metal-free N₂ reduction electrocatalyst via low-temperature plasma bombardment technology. When exclusively using ¹H NMR measurement with N₂ gas as a quantitative test method, the defect-rich Bi(110) nanoplates achieved a ¹⁵NH₃ production rate of 5.453 μg mg⁻¹ h⁻¹ and a Faradaic efficiency (11.68% at -0.6 V vs. RHE) in aqueous solutions at ambient conditions.

Electroreduction of N₂ to NH₃ under ambient conditions, especially powered by renewable sources, provides a 'clean' strategy to replace the power-consuming Haber-Bosch process for 'green' NH₃ synthesis with the aim to replace fossil fuel feedstocks and feed more of the global population for sustainable development.^[1] The N₂ reduction reaction (N₂RR), theoretically treated under ambient conditions and using water as a hydrogen source, has been proposed as a sustainable alternative for NH₃ production to alleviate the problems of environmental pollution and reduce greenhouse gas emissions. The critical bottleneck lies in the adsorption and

activation of inert N₂.^[2]

Recently, amounts of electrocatalysts (e.g., Au, Pd, Rh, etc.)^[3] have been shown to occur under ambient conditions in aqueous media, but the electrochemical performances are still very poor because most transition metals favour competitive adsorption of H⁺ over N₂.^[4] Aside from this, the scarcity and subsequent high cost lead to that their long-term usability is problematic. The design principle for N₂RR catalysts that can tune a complex, multi-step, 6-electron process remains unclear.^[5] Thus developing of highly efficient and selective electrocatalyst to obtain key products of N₂ reduction for reducing the high over-potential is extremely challenging.

The semimetal bismuth (Bi) might be a promising candidate in N₂RR due to its poor binding with H-adatoms. However, as a VA group element, its stable valence electronic structure is unfavourable for N₂ adsorption and activation. Fortunately, the electronic properties of Bi is modulated through specific synthetic method, Bi(110) nanoplates with a high fraction of isolated Bi vacancies are fabricated using a low-temperature plasma bombardment technology on Bi₂O₃ nanoplates (Figure 1A). These defect-rich Bi(110) nanoplates show a high faradaic efficiency of 11.68% at -0.6 V vs. RHE, and a ¹⁵NH₃ production rate of 5.453 μg mg⁻¹ h⁻¹ (2.400 μg h⁻¹ cm⁻² normalized by roughness factor) at -0.9 V vs. RHE under ambient conditions in aqueous solution. Rigidly speaking, it is the first time using ¹H NMR measurement with ¹⁵N₂ or ¹⁴N₂ gas as a quantitative test method for all data in aqueous electrolytes.

The X-ray diffraction (XRD) pattern (Figure 1B), scanning electron microscopy (SEM), transmission electron microscopy (TEM), atomic force microscopy (AFM) image and X-ray photoelectron spectroscopy (XPS) demonstrated that Bi₂O₃ nanoplates precursor with a thickness of 5-6 nm (Figure S1) was successfully fabricated. And its high-resolution transmission electron microscopy (HRTEM) image shows a planar spacing of 0.319 nm, corresponding to the (111) facet of Bi₂O₃.

- [a] Yue Wang, Miao-miao Shi, Fan-lu Meng, Yi-tong Zhou, Kai-hua-Liu, Yan Zhang, Zhi-wen Chen, Prof. Jun-min Yan, Prof. Qing Jiang
Key Laboratory of Automobile Materials, Ministry of Education and Department of Materials Science and Engineering
Jilin University
Changchun 130012, Jilin, China.
E-mail: junminyan@jlu.edu.cn
- [b] Di Bao, Qi Zhang, Jia-zhi Wang, Xin-bo Zhang
State Key Laboratory of Rare Earth Resource Utilization
Changchun Institute of Applied Chemistry, Chinese Academy of Sciences
Changchun 130022, Jilin, China.
- [c] Da-peng Liu, Yu Zhang
Key Laboratory of Bio-Inspired Smart Interfacial Science and Technology of Ministry of Education School of Chemistry
Beihang University
Changchun 130012, Jilin, China. Beijing 100191, China.
- [d] Jingguang G. Chen
Department of Chemical Engineering
Columbia University
New York, NY 10027, USA
E-mail: jgchen@columbia.edu
- [e] Zheng Jiang, Mi Luo
Shanghai Institute of Applied Physics, Chinese Academy of Sciences
Beijing 100080, China.
- [f] Lin Gu, Qing-hua Zhang
Institute of Physics, Chinese Academy of Sciences
Beijing 100080, China.
- [g] Xing-zhong Cao
Institute of High Energy Physics, Chinese Academy of Sciences
Beijing 100049, China.
- [h] Yao Yao, Min-hua Shao
Department of Chemical and Biological Engineering, Hong Kong University of Science and Technology
Hong Kong, 999077, China.
- [†] These authors contributed equally to this work.

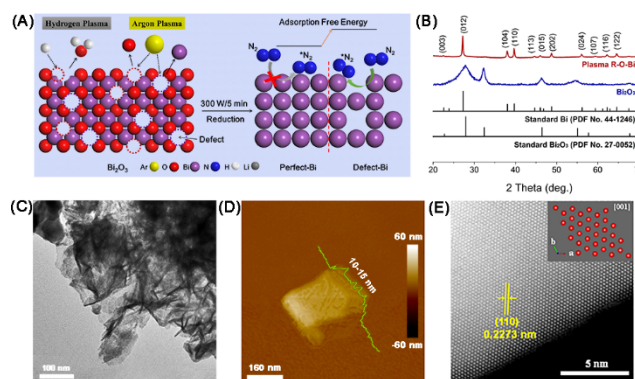


Figure 1. Characterization of Bi₂O₃ and Plasma R-O-Bi nanoplates. A) Schematic illustration of the synthesis of defect-rich Bi nanoplates and application for N₂RR. B) XRD patterns of Bi₂O₃ and Plasma R-O-Bi. C) TEM image, D) AFM image and E) HRTEM image and the corresponding atomic configuration models (inset) of Plasma R-O-Bi.

The Bi catalyst with preferentially exposed Bi(110) facets and abundant lattice defects is prepared from oxide precursors with the assistance of low-temperature plasma bombardment, as illustrated from the scheme (Figure 1A). In order to shed light on the microstructure of defect-rich Bi nanoplates (denoted as Plasma R-O-Bi), some related characterization tests were also carried out. The XRD pattern confirms hexagonal Bi (PDF No. 44-1246, Figure 1B) of Plasma R-O-Bi with a partially preserved porous nanoplate structure indicated in the SEM and TEM characterizations. (Figure 1C and Figure S2). The AFM measurements verify a rough surface and thickness in the range of approximately 10–15 nm for Plasma R-O-Bi (Figure 1D). The Bi(110) square lattice is confirmed in the high-angle annular dark-field (HAADF) image (Figure 1E), with a lattice spacing of 0.227 nm. The Brunauer-Emmett-Teller (BET) surface area and Barrett-Joyner-Halenda (BJH) pore-size distribution of Plasma R-O-Bi are determined by N₂ adsorption-desorption measurements (Figure S3). The relevant isotherms indicate that the specific surface area of Plasma R-O-Bi is smaller than that of its parent Bi₂O₃ nanoplates (declining to 43.052 m² g⁻¹ from 63.660 m² g⁻¹), which can be attributed to the much higher molecular weight of Bi than that of O and the increase in the thickness despite the larger pore sizes and additional exposed inner surface derived from efficient plasma engraving.

To further determine the electrocatalytic N₂ reduction ability of the defective Bi nanoplates, electrocatalytic N₂RR measurements are performed. The amount of NH₃ generated in the electrochemical process can be quantified from the presence of ¹⁴NH₄⁺ and ¹⁵NH₄⁺ using ¹H-NMR (Figure S4). Linear sweep voltammetry (LSV) measurements are firstly performed under N₂- and Ar-saturated Na₂SO₄ solutions to confirm the onset electrochemical potential of the N₂RR (Figure 2A). The LSV curves have the same shape but an increased current density below -0.5 V vs. RHE under the N₂ atmosphere, indicating the reaction of N₂ to NH₃ occurred. And then chronoamperometry tests are then carried out at potentials from -0.5 to -1.0 V vs. RHE to explore the catalytic activity and optimized potential of Plasma R-O-Bi catalyst for electrochemical N₂RR (Figure S5). The FE values and corresponding NH₃ production rates at different applied potentials for Plasma R-O-Bi catalyst are calculated based on the ¹H-NMR spectra under labelled ¹⁵N₂ gas (Figure S6). The total current density increases from approximate 0.051 to more than 3.658 mA cm⁻², as the potential shifts from -0.5 to -1.0 V (Figure S5B). The FE value at the applied potential of -0.5 V is 6.25% (Figure 2B), which may be caused by the low production rate owing to the low current density. With the applied potential shift to -0.6 V, the value reaches the maxima of 11.68%. Unexpectedly, the FE values decrease obviously as the applied potentials being more negative from -0.6 V due to the increase in the competing hydrogen evolution reaction (HER) (as detected by gas chromatography, Figure S7). We then calculate the production rates of NH₃ (Figure 2C), the value over Plasma R-O-Bi increases as the potential declines and reaches the highest average value of 5.453 μg mg⁻¹ h⁻¹ at -0.9 V vs. RHE, and no N₂H₄ by product is detected over the entire electrocatalytic potential range.

On the basis of the aforementioned results, blank experiment for 0.2 M Na₂SO₄ electrolyte has been done firstly to verify the safety of the test environment. No doubt, the NMR spectrum result shows that the test environment is guaranteed. Immediately, the tests without catalyst are executed to figure out

if the conductive substance of XC-72 will influence the accuracy of NMR results, undoubtedly, there is no signal detected. Most importantly, test in the absence of ¹⁴N₂ or ¹⁵N₂ (Argon instead) (Figure 2E, Table S1) is conducted to demonstrate that the N₂RR actually occurs rather than impurities in the air causing the results.^[1d,6] A blank experiment on whether applying a potential to nitrogen reduction is prerequisite or not is further implemented. All the results show that the N₂ and electrical energy are necessary for N₂RR. Then, in situ electrochemical ATR-FTIR spectroscopy was respectively recorded in N₂- and Ar-saturated Na₂SO₄ solution via the cyclic voltammogram (CV) segments of Plasma R-O-Bi catalyst with a scan rate of 2.5 mV s⁻¹, and the spectrum at -0.2 V was used as a reference. Indicated by the observed spectrum (Figure S8), the upward IR bands at ~1450 cm⁻¹ can be attributed to the H-N-H bending absorption on Plasma R-O-Bi catalyst as the applied potentials being decreased,^[3d] demonstrating the realization of N₂ protonation reaction for Plasma R-O-Bi catalyst.

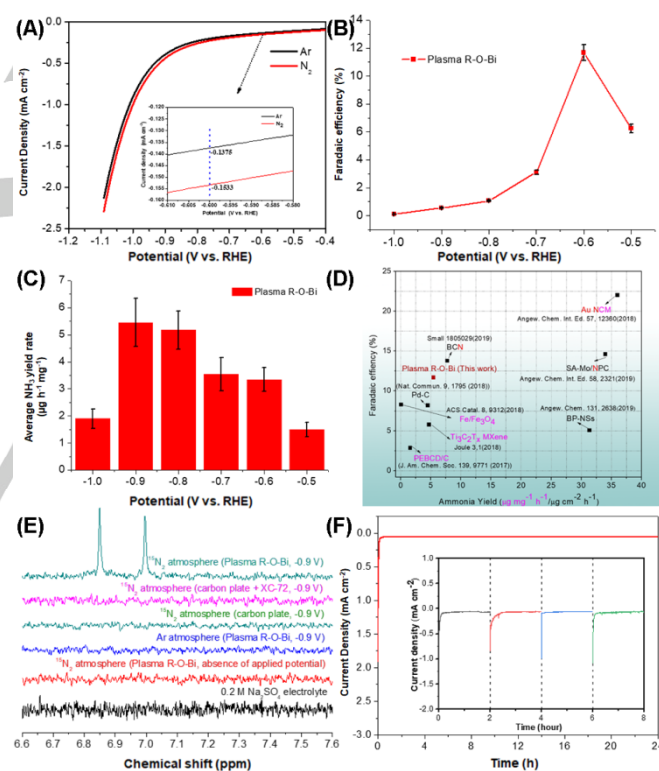


Figure 2. Performance of electrocatalytic N₂RR. A) Linear sweep voltammograms of Plasma R-O-Bi catalyst in N₂-saturated (red line) and Ar-saturated (black line) 0.2 M Na₂SO₄ aqueous solution, respectively. The details at -0.6 V is amplified (inset) B) FE for different catalysts at each given potential in a ¹⁵N₂-saturated 0.2 M Na₂SO₄ aqueous solution. C) The average NH₃ yield for different catalysts at each given potential. D) Comparison of the properties reported recently referred to the NMR tests qualitatively and partly quantitatively. E) ¹H-NMR spectra of ¹⁵N₂ and blank experiments in concentrated Na₂SO₄ aqueous solution under various conditions. F) Chronoamperometry results for Plasma R-O-Bi at the potential of -0.6 V vs. RHE under consecutive recycling electrolysis in 0.2 M Na₂SO₄ aqueous solution.

During long-term electrocatalytic tests at the applied potential of -0.6 V vs. RHE, Plasma R-O-Bi shows an ignored current density decay over 24 hr (Figure 2F). The initial current density appears slightly stable after electrolyzing for about 15 min with a

value of 0.058 mA/cm², and then gradually stabilized at 0.053 mA/cm² at about 25 min for a current density decay of 8.6%, then keep stable after 24 hr. The stability is further confirmed by XRD characterization (Figure S9), and no significant change in peak position is occurred, indicating Plasma R-O-Bi catalyst is still retained. To acquire the information of microstructure of Plasma R-O-Bi after electrolysis, a TEM technique is implanted (Figure S10), the nanoplates like morphology is preserved, including the (110) facet.

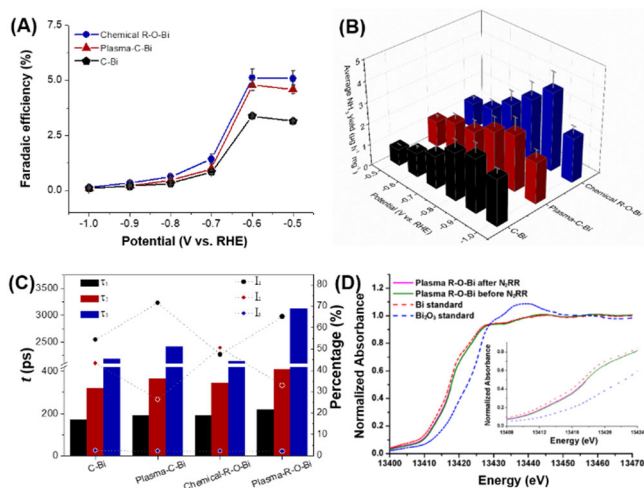


Figure 3. Performance of comparative catalysts. A) FE for different catalysts at each given potential in a ¹⁴N₂-saturated 0.2 M Na₂SO₄ aqueous solution. B) The average NH₃ yield for different catalysts at each given potential. C) Positron annihilation data for C-Bi, Plasma C-Bi, Chemical R-O-Bi and Plasma R-O-Bi. D) Bi L_{III}-edge XANES spectra of Plasma R-O-Bi before (green curve) and after (pink curve) N₂RR, commercial Bi standard (red dashed curve) and Bi₂O₃ standard (blue dashed curve).

To clarify the cause of the catalytic activity and selectivity of Plasma R-O-Bi, comparative samples, including pristine Bi₂O₃ nanoplates chemically reduced by NaBH₄ to Bi metal, commercial Bi particles and their derivatives treated with plasma etching, are also prepared and characterized as Chemical R-O-Bi, C-Bi, and Plasma C-Bi, respectively. We further test the performance of different catalysts (Figure S11), the FE values of NH₃ formation over Plasma R-O-Bi (11.68% at -0.6 V vs. RHE) is much higher than that obtained with Chemical R-O-Bi (3.729%), Plasma C-Bi (2.649%) and C-Bi (2.565%), indicating that Plasma R-O-Bi has the best selectivity for N₂RR (as shown in Figure 3A). In addition, to compare the ammonia yield rate in a most advantageous expression, the geometric area is divided. Through the analysis of the results (Figure S12), a maxima of 2.727 µg h⁻¹ cm⁻² at -0.9 V vs. RHE is obtained for Plasma R-O-Bi, higher than Chemical R-O-Bi (1.864 µg h⁻¹ cm⁻²), Plasma C-Bi (1.324 µg h⁻¹ cm⁻²) and C-Bi (1.282 µg h⁻¹ cm⁻²).

To further decode the origin of the increased N₂RR activity for Plasma R-O-Bi catalyst, electrochemical active surface areas are measured for the samples via electrochemical double-layer capacitance (C_{dl}), here we refer to Feng's paper about the concept of roughness factors (RF). In which the inherent activity (surface area normalized) can thus be acquired to exclude the effects of surface roughness.^[7] Supposed C-Bi catalyst possessed the RF of 1, we can calculate the approximate RF value of other catalysts in the light of C_{dl} processed by CV data (Figure S13). Therefore, active surface-area normalized NH₃

yield rates (normalized R_{NH₃}) for all catalysts can be calculated. As indicated from the calculated results (Figure S14), the normalized R_{NH₃} of the Plasma R-O-Bi catalyst (2.400 µg h⁻¹ cm⁻²) is still higher than other compared catalysts, specified an increase of the intrinsic activity.

The structural and compositional characterizations including HRTEM and XRD indicate the conversion of Chemical R-O-Bi from Bi₂O₃, and the morphology and phase of the commercial Bi remained nearly the same by plasma engraving (Figure S15). To quest the inherent and underlying mechanism, Positron annihilation spectrometry^[8] and X-ray absorption fine structure (XAFS)^[9] measurements are performed to characterize the defect level and types, as well as the induced change in electronic properties. Plasma R-O-Bi has a higher proportion of the short positron annihilation lifetime (τ₁) than the other samples, and the increase in τ₁ is assigned to the lattice-isolated Bi vacancy defect (Figure 3C). An increase in τ₁ is also observed for Plasma C-Bi, indicating more lattice vacancies than those in C-Bi and the key role of the plasma treatment in creating the lattice vacancies. In contrast, the other samples have a higher proportion of the longer lifetime component (τ₂) due to large defect clusters and the longest lifetime component (τ₃) due to large voids (nanoscale). The X-ray absorption near edge structure (XANES) data at the Bi L_{III}-edge of Plasma R-O-Bi, C-Bi and Bi₂O₃ nanosheet precursor are recorded at room temperature in the fluorescent mode, and the absorption edge position is defined as the energy of the inflexion point in the rising edge. The absorption edge position of Plasma R-O-Bi is closely to c-Bi, and the XANES features of Plasma R-O-Bi remain similar before and after N₂RR (Figure 3D). To ascertain quantitative structural parameters for the atoms surrounding of the central Bi atoms, we have fitted the main peaks from 1.15 to 3.6 Å for all of the samples. The structural parameters are summarized (Table S2), and the extended X-ray absorption fine structure (EXAFS) fitting curves in R-space (the fine data are displayed in Figure S16). The distance between absorber and backscatter atoms R of all the paths are fixed to their corresponding values as references, which produced a satisfactory fit with the percentage misfit (R-factor) being in 1.29% and 0.91%, respectively. To decrease the number of fitting parameters, we commonly fix the Debye-Waller factor σ² to the theoretical values (Table S2). The Bi-Bi bond coordination number of Plasma R-O-Bi is smaller than that of Bi standard, further confirming the existence of the lattice-isolated Bi vacancy defect.

The Gibbs free energy ΔG on perfect Bi and defective Bi for N₂RR is obtained from density functional theory (DFT) calculations and analysed as an effective descriptor for investigating catalytic activities and possible mechanism of N₂RR.^[10] In the entire reaction network, the protonation process to form N₂H* is the rate-determining step for converting N₂ to NH₃. As indicated by the Gibbs free energy diagrams (Figure 4A and Figure S17, Bi defect-(110) catalyse N₂ to form N₂H* under mild conditions due to its lower ΔG_{N₂H*} value than that of perfect Bi(110). And the corresponding binding strength between catalyst and N₂H* intermediate can also be inferred from the Gibbs free energy diagram. Then volcano plot of the potential-limiting steps and ΔG_{N₂H*} are constructed (Figure 4B),^[11] and the Gibbs free energy of N₂H* on Bi defect-(110) is 0.89 eV, which is closer to the peak of the volcano than that of other metals such as Pt, Pd, and Cu. Here, considering the hydrogen evolution as the main side reaction of N₂RR, we also compare the hydrogen

evolution performance of different catalysts, and Bi shows the poor activity due to its poor binding with H-adatoms (Figure 4C).^[4b,12] The DFT calculations with CI-NEB method (Figure 4D) is further conducted and revealed that the active barrier of the defect Bi(110) facet is only 0.56 eV, which is much lower than that of perfect Bi(110), indicating the favorable kinetic characteristics. Overall, our results suggest that the defect Bi(110) facet enables the surface active sites to adsorb and activate the N_2 to form adsorbed N_2H^* species with favourable N_2RR energetics, which is responsible for the superior N_2RR performance.

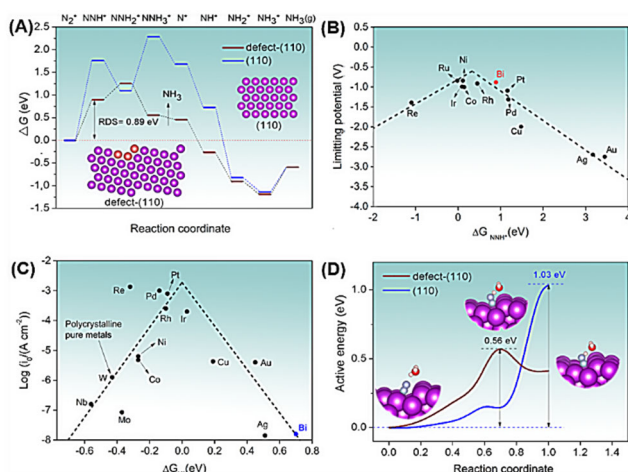


Figure 4. DFT simulations of N_2 adsorption on Bi facets. A) The free-energy diagrams for N_2RR on Bi(110) and Bi defect-(110) facets via a distal pathway. B) Limiting potentials for N_2 electroreduction on each metal against the binding energy of N_2H^* , the red dot is the Bi defect-(110) facet; comparison limiting potential data are from Ref. 11. C) Volcano plot for HER on representative transition metals; comparison data are from Ref. 4b, 12. D) The active energy of the rate-determining step.

In conclusion, the combination of theoretical and experimental strategies confirmed the key role of defects in enabling adsorption and activation of N_2 and subsequent conversion on semimetal defect-rich Bi for electrochemical reduction of N_2 to NH_3 . The defect-rich Bi(110) nanoplates show a high faradic efficiency of 11.68% and NH_3 production rate of $5.453 \mu\text{g mg}^{-1} \text{h}^{-1}$. The design principle of using defects to transform a nearly non-catalytic N_2RR material into a very robust and active catalyst indicates that strategies for achieving N_2 adsorption and activation should be further explored, and this principle represents a general strategy for the development of new heterogeneous catalytic systems for 'green' ammonia synthesis.

Acknowledgements

This work was financially supported by the National Natural Science Foundation of China (51522101 and 51631004), the National Key Research and Development Program of China (2017YFA0206700 and 2016YFB0100100), the Strategic Priority

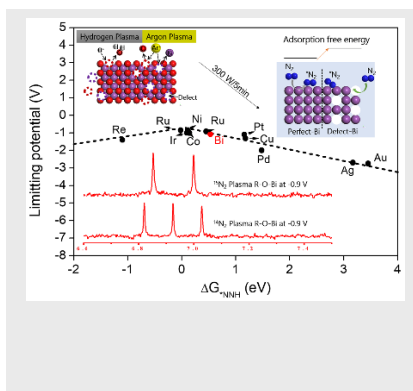
Research Program of the Chinese Academy of Sciences (XDA21010210), Program for JLU Science and Technology Innovative Research Team (2017TD-09), and the United States Department of Energy (DE-FG02-13ER16381).

Keywords: bismuth nanosheet • defects rich • nitrogen reduction • NMR quantitative test • non-noble metal

- a) J. G. Chen, R. M. Crooks, L. C. Seefeldt, K.L. Bren, R. M. Bullock, M. Y. Darensbourg, P. L. Holland, B. Hoffman, M. J. Janik, A. K. Jones, M. G. Kanatzidis, P. King, K. M. Lancaster, S. V. Lymar, P. Pfromm, W. F. Schneider, R. R. Schrock, *Science* **2018**, *360*, 6391; b) M. Falcone, L. Chatelain, R. Scopelliti, I. Živković, M. Mazzanti, *Nature* **2017**, *547*, 332-335; c) S. Chu, A. Majumdar, *Nature* **2012**, *488*, 294-303; d) C. Liu, K. K. Sakimotoa, B. C. Colón, P. A. Silverc, D. G. Nocera, *Proc. Natl. Acad. Sci. U.S.A.* **2017**, *114*, 6450-6455; e) K. Arashiba, Y. Miyake, Y. Nishibayashi, *Nat. Chem.* **2011**, *3*, 120-125.
- a) S. Gambarotta, J. Scott, *Angew. Chem. Int. Ed.* **2004**, *43*, 5298-5308; b) M. D. Fryzuk, *Science* **2013**, *340*, 1530-1531; c) M. A. Légaré, G. B. Chabot, R. D. Dewhurst, E. Welz, I. Krummenacher, B. Engels, H. Braunschweig, *Science* **2018**, *359*, 896.
- a) D. Bao, Q. Zhang, F. L. Meng, H. X. Zhong, M. M. Shi, Y. Zhang, J. M. Yan, Q. Jiang, X. B. Zhang, *Adv. Mater.* **2017**, *29*, 1604799; b) J. Wang, L. Yu, L. Hu, G. Chen, H. L. Xin, X. F. Feng, *Nat. Commun.* **2018**, *9*, 1795; c) H. M. Liu, S. H. Han, Y. Zhao, Y. Y. Zhu, X. L. Tian, J. H. Zeng, J. X. Jiang, B. Y. Xia, Y. Chen, *J. Mater. Chem. A* **2018**, *6*, 3211-3217; d) Y. Yao, S. Zhu, H. Q. Wang, H. J. Li, M. H. Shao, *J. Am. Chem. Soc.* **2018**, *140*, 1496-1501; e) L. Zhang, X. Q. Ji, X. Ren, Y. J. Ma, X. F. Shi, Z. Q. Tian, A. M. Asiri, L. Chen, B. Tang, X. P. Sun, *Adv. Mater.* **2018**, *30*, 1800191.
- a) C. X. Guo, J. R. Ran, A. Vasileffa, S. Z. Qiao, *Energy Environ. Sci.* **2018**, *11*, 45-46; b) J. K. Nørskov, T. Bligaard, A. Logadottir, J. R. Kitchin, J. G. Chen, S. Pandalov, U. Stimming, *J. Electrochem. Soc.* **2005**, *152*, J23-J26.
- J. X. Zhao, Z. F. Chen, *J. Am. Chem. Soc.* **2017**, *139*, 12480-12487.
- a) M. M. Shi, D. Bao, B. R. Wulan, Y. H. Li, Y. F. Zhang, J. M. Yan, Q. Jiang, *Adv. Mater.* **2017**, *29*, 1606550; b) T. Shima, S. W. Hu, G. Luo, X. H. Kang, Y. Luo, Z. M. Hou, *Science* **2013**, *340*, 1549-1552.
- L. Hu, A. Khaniya, J. Wang, G. Chen, W. E. Kaden, X. F. Feng, *ACS Catal.* **2018**, *8*, 9312-9319.
- a) M. L. Guan, C. Xiao, J. Zhang, S. J. Fan, R. An, Q. M. Cheng, J. F. Xie, M. Zhou, B. J. Ye, Y. Xie, *J. Am. Chem. Soc.* **2013**, *135*, 10411-10417; b) M. Reiner, A. Bauer, M. Leitner, T. Gigl, W. Anwand, M. Butterling, A. Wagner, P. Kudejova, C. Pfeleiderer, C. Hugenschmidt, *Sci. Rep.* **2016**, *6*, 29109; c) J. Dryzek, *Tribol. Lett.* **2010**, *40*, 175-180; d) Cz. Szymański, St. Chabik, J. Pajalk, B. Rozenfeld, *phys. stat. sol. (a)* **1980**, *60*, 375-380.
- a) Z. Cai, Y. M. Bi, E. Y. Hu, W. Liu, N. Dwarica, Y. Tian, X. L. Li, Y. Kuang, Y. P. Li, X. Q. Yang, H.L. Wang, X. M. Sun, *Adv. Energy Mater.* **2018**, *8*, 1701694; b) F. Boscherini, *Synchrotron Radiation* **2015**, 485-498.
- a) E. Skulason, T. Bligaard, S. Gudmundsdottir, F. Studt, J. Rossmeisl, F. Abild-Pedersen, T. Vegge, H. Jonsson, J. K. Nørskov, *Phys. Chem. Chem. Phys.* **2012**, *14*, 1235-1245; b) Z. W. She, J. Kibsgaard, C. F. Dickens, I. Chorkendorff, J. K. Nørskov, T. F. Jaramillo, *Science* **2017**, *355*, eaad4998.
- J. H. Montoya, C. Tsai, A. Vojvodic, J. K. Nørskov, *ChemSusChem* **2015**, *8*, 2180-2186.
- J. Greeley, T. F. Jaramillo, J. Bonde, I. Chorkendorff, J. K. Nørskov, *Nat. Mater.* **2006**, *5*, 909-913.

COMMUNICATION

Defect-rich Semimetal bismuth (Bi) nanoplates achieved a $^{15}\text{NH}_3$ production rate of $5.453 \mu\text{g mg}^{-1} \text{h}^{-1}$ and a higher Faradaic efficiency (11.68% at -0.6 V vs. reversible hydrogen electrode) in aqueous solutions at ambient conditions because of its poor binding with H-atoms for increasing the selectivity and production rate. In addition, we firstly use ^1H NMR measurement with N_2 gas as a quantitative test method for all data in aqueous electrolytes.



Yue Wang, Miao-miao Shi, Di Bao, Fan-lu Meng, Qi Zhang, Yi-tong Zhou, Kai-hua Liu, Yan Zhang, Jia-zhi Wang, Zhi-wen Chen, Da-peng Liu, Zheng Jiang, Mi Luo, Lin Gu, Qing-hua Zhang, Xing-zhong Cao, Yao Yao, Min-hua Shao, Yu Zhang, Xin-Bo Zhang, Jingguang G. Chen, Jun-min Yan, Qing Jiang

Generating Defect-Rich Bismuth for Enhancing Rate of Nitrogen Electroreduction to Ammonia

Accepted Manuscript